Analyst

PAPER

View Article Online
View Journal

Cite this: DOI: 10.1039/c8an02077a

Aptamer superstructure-based electrochemical biosensor for sensitive detection of ATP in rat brain with *in vivo* microdialysis

Yanan Jiang,[a,b] Wenjie Ma,[a,b] Wenliang Ji,[a] Huan Wei[a,b] and Lanqun Mao *[a,b]

Received 29th October 2018,
Accepted 31st December 2018

DOI: 10.1039/c8an02077a

rsc.li/analyst

Highly sensitive and selective sensing of ATP in rat brain has attracted increasing interest from interdisciplinary fields of analytical chemistry and neuroscience owing to the importance of ATP in cellular metabolism and signal transduction. Herein, we demonstrated an electrochemical biosensor having an aptamer superstructure as a recognition element for the selective and sensitive detection of ATP in rat brain. Unlike the electrochemical aptamer-based sensors (aptasensors) built by assembling a simple DNA structure containing only one aptamer unit onto the electrode substrate, the aptasensor described here was developed by assembling an aptamer superstructure consisting of consecutive aptamer units in DNA strands onto the electrode substrate. Each aptamer unit in the superstructure was labelled with an electrochemical probe (*i.e.*, methylene blue, MB) for signal readout. The aptamer superstructure was assembled onto the surface of a gold electrode to form the electrochemical aptasensor. In the presence of ATP, the strong electrochemical signals produced by multiple redox molecules labeled on the aptamer units clearly decreased because of the disassembling of the aptamer superstructure from the electrode surface due to strong interactions between ATP and the aptamer units. In this approach, the aptasensor was well responsive to the ATP concentration, and the current decrease was linearly related to the ATP concentration ranging from 0.1 nM to 1 mM. Moreover, the aptasensor has high selectivity and good regenerability. Due to these properties, the aptasensor with an aptamer superstructure can exhibit practical applications for ATP assay in rat brain combined with *in vivo* microdialysis.

1. Introduction

In vivo detection of physiologically important molecules continues to attract intense interest due to the essential roles of neurochemicals in brain functions.[1–5] As one of the multifunctional nucleotides, adenosine triphosphate (ATP) is known as the primary "energy currency" for most animate beings, playing a significant role in regulating various biological processes such as cellular metabolism and signal transduction.[6–9] Moreover, the level of ATP can be used as an indicator for many clinical diseases including hypoglycemia, hypoxia, ischemia, and some neurodegenerative disorders.[10–13] Therefore, developing reliable, sensitive and selective methods for ATP detection will certainly pave an effective way to understand the neurochemical mechanisms of brain functions.

Up to now, some analytical approaches have been developed for the quantitative measurement of ATP, and these include surface enhanced Raman scattering (SERS), mass spectrometry (MS), fluorescence spectrometry, bioluminescence, chemiluminescence, and electrochemical analysis.[14–20] Among these methods, the commercial ATP assay system with bioluminescence detection kit is prevalently used for the detection of ATP with a luciferin-luciferase-based assay; however, luciferase is unstable in solution with the loss of biological activity.[21] Although these methods have been used for ATP sensing, it remains a great challenge to selectively and sensitively detect ATP in rat brain because of the complexity of the cerebral system and the low concentration for the basal level of ATP. In this case, the key factors for ATP sensing in the cerebral system should be integration of ATP recognition elements with signal enhancement protocol.

Aptamers are single-stranded DNA or RNA molecules isolated from a random sequence nucleic acid pool by an *in vitro* selection technique termed as systematic evolution of ligands by exponential enrichment (SELEX); over the past few decades, they have received substantial attention due to the merits of high affinity and specificity.[22–26] Compared with conventional

[a]*Beijing National Laboratory for Molecular Sciences, Key Laboratory of Analytical Chemistry for Living Biosystems, Institute of Chemistry, the Chinese Academy of Sciences (CAS), CAS Research/Education Center for Excellence in Molecule Science, Beijing 100190, China. E-mail: lqmao@iccas.ac.cn; Fax: +86-10-62559373*
[b]*University of Chinese Academy of Sciences, Beijing 100049, China*

affinity reagents such as antibodies and enzymes, aptamers are advantageous in terms of synthesis convenience, design flexibility, and chemical stability.[27–30] Owing to these unique features, aptamers have been utilized in molecular imaging, drug delivery, and biochemical research with a broad range of targets including metal ions, small molecules, and even cells.[31–37] Generally, aptamer-based biosensors are primarily based on conformational transitions induced by the targets, where the signal can be monitored by fluorescence, colorimetry, and electrochemical methods.[38–40] For instance, aptamer-conjugated nanoparticles can be used for the selection and detection of cancer cells *via* fluorescent imaging and flow cytometry. The aptamer sequence is selected using a cell-based SELEX strategy, allowing specific recognition of the cells from complex mixtures even for whole blood samples.[41] Among the strategies employed for the development of aptasensors, electrochemical methods have been primarily used because of the operational convenience and low fabrication cost as well as high sensitivity. Recently, a promising dual-reporter approach was demonstrated to perform a baseline drift correction for electrochemical aptasensors that deploy directly into flowing whole blood, reducing the drift from up to 50% to less than 2% under challenging conditions.[42] Our group fabricated polyimidazolium-modified micropipettes with ion current rectification at a micrometer scale; we then further developed this into a sensing platform for ATP based on the interaction between aptamer and ATP.[43,44] Moreover, we used aptamer-complementary DNA oligonucleotides as the probes to prepare electrochemical aptasensors with a ready regeneration feature,[45,46] which can be further optimized with an azobenzene moiety embedded into the DNA chain by UV light irradiation for more than seven cycles.[47] Nevertheless, these strategies using single aptamer as the recognition element still have limitations in signal gain and corresponding sensitivity. In this context, a DNA superstructure was prepared with one single-stranded DNA probe hybridized with two probes through each complementary region to form long concatamers. These concatamers containing multiple signal probes can be used as excellent sensing units because the superstructure can improve the sensitivity of aptasensors.[48–54]

Herein, we demonstrated an electrochemical aptasensor for the selective detection of ATP in the cerebral system based on signal amplification with aptamer superstructures (Scheme 1). In the absence of ATP, the electrode modified with a long aptamer superstructure showed a strong electrochemical signal because of the presence of multiple redox molecules on the sequence (A). In the presence of ATP, the aptamer superstructure disassembled through aptamer-target interactions, resulting in decrease in the electrochemical signal (B). This resulted in the sensing mechanism for the aptamer superstructure-based aptasensor. The aptasensor was responsive to ATP with high selectivity and directly detected ATP in the rat brain when combined with *in vivo* microdialysis.

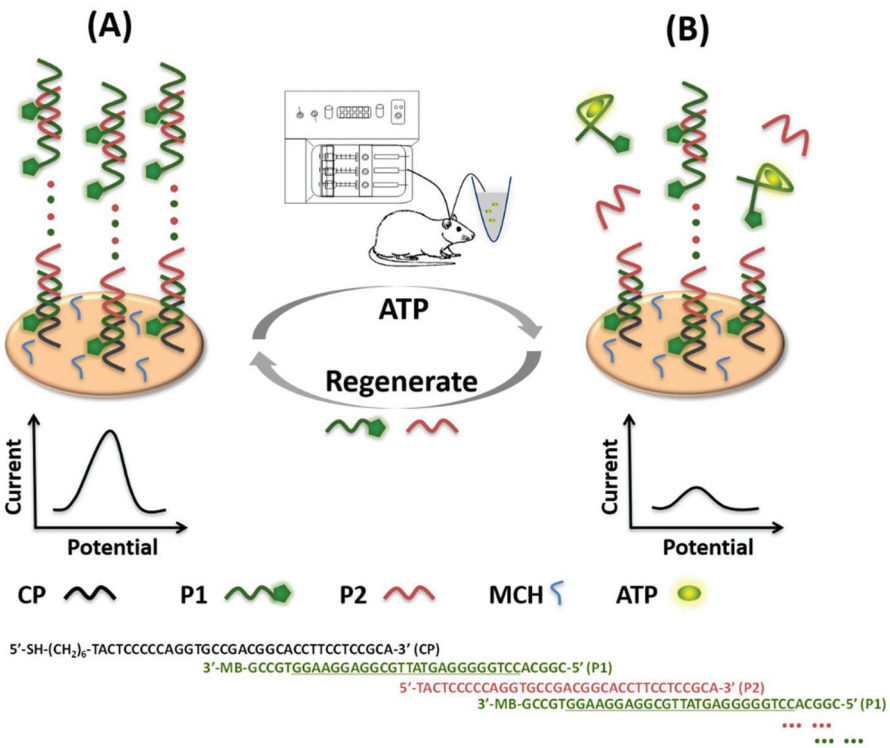

Scheme 1 Schematic illustration of the detection of ATP in rat brain microdialysate with the aptasensor based on the aptamer superstructure. The marked sequences in probe 1 (P1) are the aptamer sequences for ATP.

2. Experimental

2.1. Reagents and solution

DNA oligonucleotides were synthesized and purified with HPLC by Takara Biotechnology (Dalian, China). Adenosine 5′-triphosphate (ATP) disodium salt hydrate, adenosine 5′-diphosphate (ADP) disodium salt, adenosine 5′-monophosphate (AMP) disodium salt, thymidine 5′-triphosphate (TTP) sodium salt, uridine 5′-triphosphate (UTP) trisodium salt dihydrate, guanosine 5′-triphosphate (GTP) sodium salt hydrate, cytidine 5′-triphosphate (CTP) disodium salt, ATP hydrolase (Apyrase), mercaptohexanol (MCH), tris(2-carboxyethyl)phosphine hydrochloride (TCEP), and tris(hydroxymethyl)aminomethane (Tris) were all purchased from Sigma-Aldrich. Potassium ferricyanide ($K_3Fe(CN)_6$) was obtained from Beijing Chemical Company (Beijing, China). Artificial cerebrospinal fluid (aCSF, pH 7.4) was prepared by mixing NaCl (126 mM), KCl (2.4 mM), KH_2PO_4 (0.5 mM), $MgCl_2$ (0.85 mM), $NaHCO_3$ (27.5 mM), Na_2SO_4 (0.5 mM), and $CaCl_2$ (1.1 mM) in water, which was used as the perfusion solution for *in vivo* microdialysis. All other reagents were of at least analytical grade and used as received without further purification. All solutions were prepared with ultrapure water (18.2 MΩ cm) from a Milli-Q system.

2.2. Apparatus and electrochemical measurements

Electrochemical measurements were performed with a computer-controlled CHI 730D electrochemical workstation (Shanghai, China) at room temperature. A conventional three-electrode electrochemical cell was used with functionalized gold electrodes (Au, 2 mm in diameter) as the working electrode, a platinum wire as the counter electrode, and an Ag/AgCl electrode (KCl-saturated) as the reference electrode. Cyclic voltammetry (CV) was performed within a potential range from −0.2 to 0.6 V at a scan rate of 100 mV s^{-1}. Electrochemical impedance spectra (EIS) were obtained in Tris-HCl buffer (10 mM, pH 7.4) containing 0.1 M KCl and 5.0 mM $[Fe(CN)_6]^{3-/4-}$ (1 : 1) mixture as the redox probe in a frequency range from 0.1 Hz to 10 kHz with 5 mV as the amplitude. Alternating current voltammetry (ACV) was carried out in Tris-HCl buffer (10 mM, pH 7.4) containing 0.1 M NaCl and 1 mM $MgCl_2$ in a potential range from −0.15 to −0.4 V (*vs.* Ag/AgCl), potential step of 0.001 V, amplitude of 0.05 V and frequency of 60 Hz. The ACV shown was baseline subtracted by setting all curves to 0 at −0.15 V, which is distant from the redox peak of MB.[55]

2.3. Gel electrophoresis

Gel electrophoresis was performed by placing the samples on 2% agarose gels containing 0.1 μL Gel-Red dye per milliliter of gel volume in 1× TAE buffer (40 mM Tris acetate, 1 mM EDTA, pH 8.3). The samples were prepared and kept for 12 hours at room temperature. The gel was run at a constant voltage of 90 V for 40 minutes followed by imaging using a Gel-Pro ZF-288 system (Shanghai, China).

2.4. Preparation of electrochemical aptasensor

Au electrodes were first polished with alumina powders (0.3 and 0.05 μm in diameter) on microcloth sequentially, followed by ultrasonic cleaning in ethanol and ultrapure water each for 5 minutes to remove residual Al_2O_3. The electrodes were then electrochemically cleaned by potential scanning from −0.2 to 1.6 V at 0.1 V s^{-1} for 20 cycles in 0.5 M H_2SO_4 solution. After that, the electrodes were rinsed with water and dried with nitrogen. Prior to immobilization onto the gold electrode surface, the capture probe (CP, structure shown in Scheme 1) was dissolved in Tris-HCl buffer (10 mM, pH 7.4, containing 0.1 M NaCl and 1 mM $MgCl_2$) with 10 mM TCEP and incubated in the dark for 1 h to reduce disulfide bonds. Then, the CP solution (1 μM) was dropped onto the cleaned Au electrode surface for 10 h to form Au–S bonds in a humidified chamber. The electrode was further immersed in 2 mM MCH solution to modify the uncovered gold electrode surface. To prepare the aptamer superstructure, probe 1 (P1) and probe 2 (P2) (1 μM) solutions were dropped onto the electrode surface with CP grafted for 10 h. For the detection of ATP, the aptamer superstructure-modified electrode was incubated in equal volumes of different concentrations of target ATP or non-target molecule solutions for 10 minutes at room temperature. After each step, the electrode was washed with Tris-HCl buffer and dried under nitrogen gas. Before the electrochemical measurements, the electrodes were incubated in Tris-HCl solution.[51,56]

2.5. *In vivo* microdialysis and microdialysate ATP sensing

In vivo microdialysis was performed using a previously reported process, and all animal procedures were performed in accordance with the Guidelines for Care and Use of Laboratory Animals of National Center for Nanoscience and Technology of China and approved by the Animal Ethics Committee of National Center for Nanoscience and Technology of China.[18,44] Briefly, adult male Sprague-Dawley rats (250–300 g) were housed with food and water *ad libitum* according to a 12:12 h light–dark schedule. Through the standard stereotaxic system, a microdialysis guide cannula (BAS/MD-2250, Indiana, America) was implanted into the brain cortex (AP = 0 mm, L = 2.58 mm from bregma, V = 0.25 mm from dura). The guide cannula was fixed with three skull screws and dental cement. After the insertion of the microdialysis probe, stainless steel dummy blockers were inserted into the guide cannula and fixed. The animals' body temperature was kept at 37 °C using a heating pad throughout the surgery. The rats were allowed to recover for at least 24 h; then, a microdialysis probe (BAS) with dialysis length of 4 mm, diameter of 0.24 mm, and cutoff of 20 kDa was implanted into the rat cortex. Before the microdialysate was collected for analysis, the probe was continuously perfused with artificial cerebrospinal fluid (aCSF) at 1 μL min^{-1} for at least 90 min to reach equilibration. The rat cortex microdialysate was then used for ATP sensing.

3. Results and discussion

3.1. Design and construction of the aptasensor for ATP sensing

Scheme 1 illustrates the mechanism of the ATP aptasensor based on signal amplification with DNA superstructures. To prepare the aptasensor, a thiolated capture probe (CP) was initially confined onto the Au electrode surface through the formation of Au–S bonds. Then, MCH was modified onto the uncovered gold electrode surface. To construct the aptamer superstructure, ssDNA probes P1 and P2 were added to the environmental solution. Starting from the modified CP on the electrode surface, multiple concatenated units of P1 (35-mer) and P2 (35-mer) containing partially complementary sequences (17-mer) were hybridized with CP. Then, the consecutive DNA-hybridized assemblies were created on the electrode surface with repeating units of P1 and P2. The DNA modification and assembly strategy was similar to a previously reported process.[51,57] In this system, P1 was labeled with MB, which exhibited good electrochemical properties and produced strong electrochemical signals. P1 contained the aptamer sequence of ATP in the sequence-designed DNA assemblies. In the presence of ATP, the DNA superstructure gradually disassembled due to the strong binding between ATP and its aptamer, leading to the dissociation of P1 from the electrode surface and thus to the reduction in MB signals.

The fabrication procedures for the ATP aptasensor were characterized by cyclic voltammetry (CV) and electrochemical impedance spectroscopy (EIS), which are effective tools to obtain information about the interface properties of surface-modified electrodes.[58] Fig. 1 shows the cyclic voltammograms (CVs) of the sensors prepared with different stages with $[Fe(CN)_6]^{3-/4-}$ as the redox probe. For bare Au electrode, we observed a couple of reversible redox peaks of $[Fe(CN)_6]^{3-/4-}$. The immobilization of the capture probe (CP) and surface-blocking molecules of MCH effectively decreased the current responses of $[Fe(CN)_6]^{3-/4-}$ on the modified electrode due to the negative charges on the DNA backbone and MCH. After CP hybridized with P1 and P2 to form the DNA superstructure, the current further decreased because more negative charges were created by the dsDNA polymers on the electrode surface. In the presence of ATP molecules, the binding of ATP to P1 melted the DNA concatamers and restored the peak current to the initial value obtained for the CP/MCH-modified electrode.

In the Nyquist plot of EIS, the diameter of the semicircle at high frequencies corresponds to the interfacial electron transfer resistance (R_{et}), and the change in the diameter reflects the change in R_{et} with different modified electrodes. As shown in Fig. 1B, a small semicircle domain (black squares) was observed for the bare Au electrode, suggesting a fast electron transfer process of $[Fe(CN)_6]^{3-/4-}$. A significant semicircle (red circles) with enhanced electron transfer resistance was observed after the immobilization of CP and MCH on the electrode surface. R_{et} continued to increase when the DNA superstructure was formed with repetitive units of P1 and P2. However, R_{et} decreased significantly after ATP treatment because of the disassembly of the DNA superstructure. The EIS results were consistent with the CV observations, and both experiments revealed that the aptasensor was successfully fabricated with the DNA superstructure.

3.2. Linearity, selectivity and regeneration ability of the aptasensor

To quantitatively investigate ATP concentrations based on the effect of ATP molecules and DNA superstructure, ACV responses were used to record the reduction current of MB in the sensing system, where the initial current value without ATP was defined as I_0. As shown in Fig. 2A, the peak current (I) of MB decreased significantly with increasing ATP concentration (from 0.1 nM to 10 mM). Through the analysis of the correlation between the current signal change ($\Delta S = 1 - I/I_0$) and the concentration of ATP, a linear relationship was obtained with the logarithm of ATP concentrations from 0.1 nM to

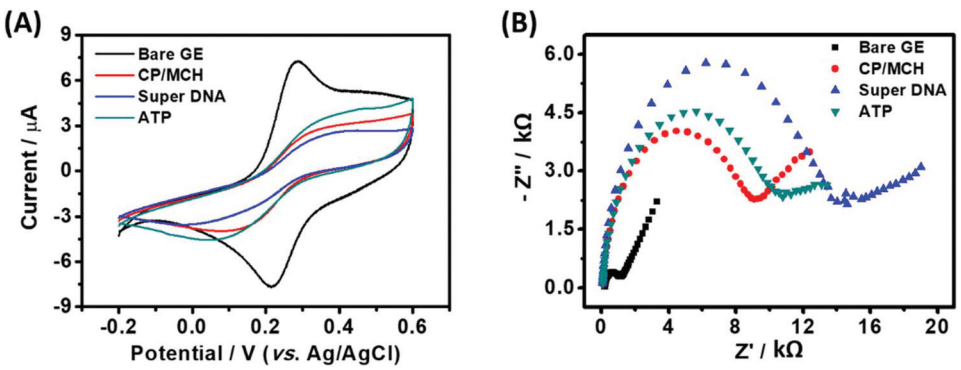

Fig. 1 (A) Typical CVs recorded with Au electrodes before (black curve) and after the electrodes were modified with CP (1 μM) and MCH (2 mM) (red curve), aptamer superstructure (1 μM) (blue curve). The dark green curve represents CV recorded with the aptasensor after the aptasensor was treated in ATP solution (1 mM). Electrolyte, Tris-HCl buffer (10 mM, pH 7.4) containing 0.1 M KCl and 5.0 mM $[Fe(CN)_6]^{3-/4-}$. Scan rate, 0.1 V s^{-1}. (B) EIS recorded with the same electrodes as those used in (A) under the same experimental conditions. The frequency range was 0.1 Hz to 10 kHz with 5 mV as the amplitude.

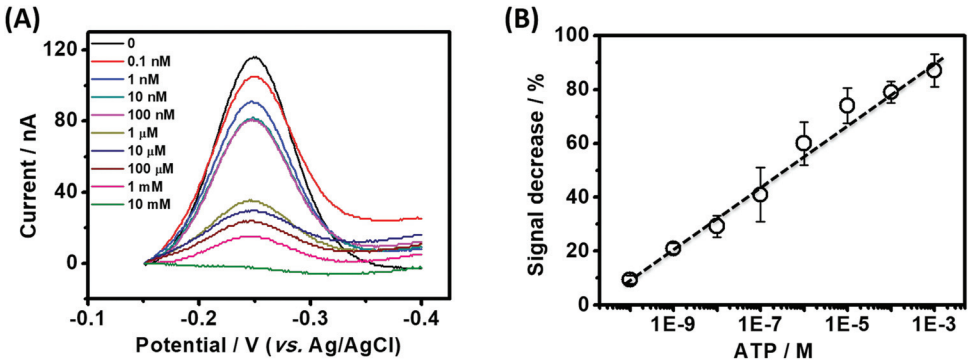

Fig. 2 (A) Alternating current voltammograms (ACVs) recorded with the aptasensors in Tris-HCl buffer (10 mM, pH 7.4) containing 0.1 M NaCl and 1 mM $MgCl_2$ after the sensors were incubated for 10 minutes in ATP solutions with different concentrations (0 (black), 0.1 nM (red), 1 nM (blue), 10 nM (dark green), 100 nM (magenta), 1 μM (dark yellow), 10 μM (navy), 100 μM (wine), 1 mM (pink), 10 mM (olive)). (B) Plots of the peak current signal change ($\Delta S = 1 - I/I_0$) *versus* ATP concentration. The dashed line indicates a linear relationship between the peak current change and the logarithm of the ATP concentration. The error bars represent the standard deviation from three independent measurements.

1 mM ($\Delta S = 20.87 + 11.59 \log C_{ATP}$ (nM) ($R^2 = 0.994$)); the limit of detection was 50 pM.

In addition to sensitivity, the selectivity of the aptasensor is another critical parameter for cerebral analysis owing to the chemical complexity of the cerebral system. From the gel electrophoresis results (Fig. 3A), we inferred that high-molecular-weight DNA concatamers with repeating units of hybridized P1 and P2 were formed. The analysis displayed a ladder of different lengths of the DNA concatamers with the maximum length of more than 600 base pairs. Once ATP was added into the hybridized solution, the DNA superstructures disassembled, as shown in Fig. 3A (lane 5). However, no evident change was found after the treatment with the other two types of adenosine nucleosides (*i.e.*, ADP and AMP) or the analogue NTPs (*i.e.*, TTP, GTP, CTP and UTP). The gel electrophoresis results shown in Fig. 3A were consistent with the ACV responses recorded with the aptasensors, and these ACV responses remained almost unchanged after the aptasensors were treated with ATP analogues even though the concentrations of the ATP analogues (1 mM) were higher than that of ATP (1 μM) (inset, Fig. 3B). These results demonstrated

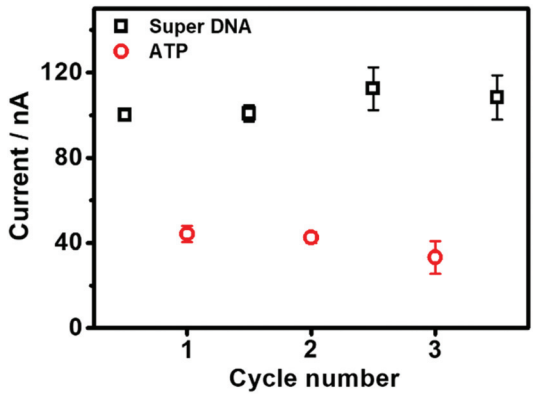

Fig. 4 Regeneration of the ATP aptasensor by alternatively treating the aptasensors with ATP and hybridizing with DNA probes. The current signal was recorded with the aptamer superstructure (black square) and after the aptasensors were treated with ATP (red circle). The concentration of ATP used for the disassembly of the aptamer superstructure was 1 μM, and that for the hybridized P1 and P2 was 1 μM for each cycle. The ACV conditions were the same as those in Fig. 2A. The error bars represent the standard deviation from three independent measurements.

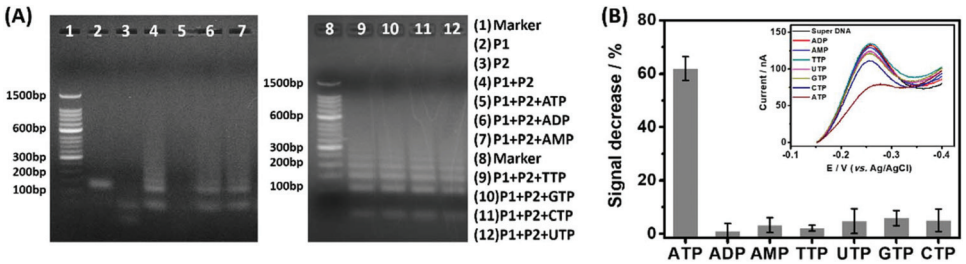

Fig. 3 (A) Gel electrophoresis results of the superstructures before (lane 4) and after separate treatments with ATP (lane 5), ADP (lane 6), AMP (lane 7), TTP (lane 9), GTP (lane 10), CTP (lane 11) and UTP (lane 12). The DNA superstructure almost disappeared when it was treated with ATP (lane 5). The other lanes are biomarkers (lane 1 and 8), probe 1 (lane 2) and probe 2 (lane3). (B) Histogram of electrochemical signal changes toward different target treatments under the same conditions. Inset: ACVs recorded with the aptasensors before and after the aptasensors were treated with different targets. ACV conditions were the same as those in Fig. 2A. The aptasensors were separately treated with ADP (1 mM), AMP (1 mM), NTPs (concentration for each NTP was 1 mM) and ATP (1 μM) for 10 minutes. The error bars represent the standard deviation from three independent measurements.

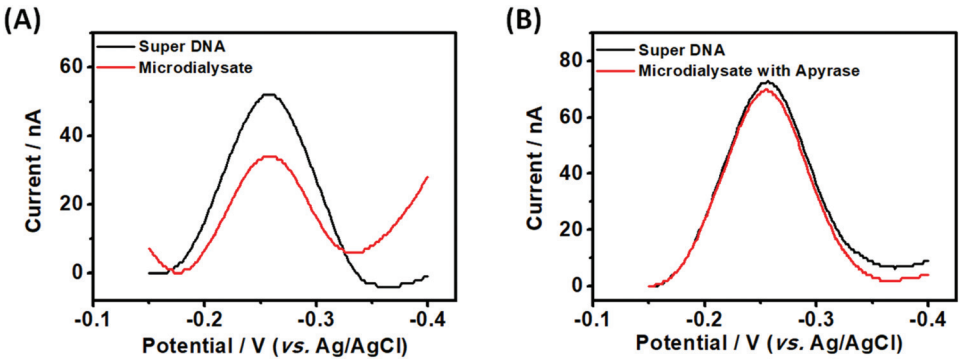

Fig. 5 (A) Typical ACVs obtained with the aptamer superstructure-based aptasensor before (black curve) and after (red curve) the aptasensor was treated with brain microdialysate from rat brain cortex for 10 minutes. (B) ACVs recorded for the aptasensor before (black curve) and after (red curve) the aptasensor was treated with Apyrase-treated microdialysate. The brain microdialysate (200 μl) was treated with Apyrase (1 U, one unit of Apyrase consumes 1.0 μmol of inorganic phosphate from ATP to ADP per minute at pH 6.5 at 30 °C) for 30 minutes.

that the aptasensor exhibited high selectivity for ATP detection.

Meanwhile, the regenerability of the aptasensor is another important issue for practical application. Owing to the strong chemisorbed effect between CP and the electrode surface, the sensor was allowed to regenerate after ATP treatment. The subsequent assembly probes maintained almost the same ability to form long DNA concatamers. Therefore, the electrochemical signal was readily regenerated by incubating the electrodes with P1 and P2 for 10 h after the electrodes were treated with 1 μM ATP, as shown in Fig. 4. After being challenged with ATP and regenerated, the aptasensor signal recovered almost to the original value, demonstrating that the fabricated electrochemical aptasensor is regenerable for practical applications.

3.3. ATP assay in rat brain

Fig. 5 depicts typical ACVs obtained with the aptasensor in Tris-HCl buffer before (black curve) and after (red curve) incubating the aptasensors with microdialysates from rat brain cortex. The reduction current decreased after the aptasensor was directly treated with the brain microdialysates for 10 minutes, as shown in Fig. 5A. The basal level of ATP from the cortex microdialysate was determined to be 12.0 ± 5.0 nM (n = 3), which was consistent with the reported values.[18] Due to the chemical complexity of the rat brain, we further conducted the selectivity test in brain microdialysate to validate the aptasensor's applicability for *in vivo* analysis. In this case, Apyrase was used because it selectively catalyzes the decomposition of ATP into ADP and AMP. The rat brain cortex microdialysate was primarily pretreated by Apyrase for 30 minutes. Fig. 5B shows the ACV results before (black curve) and after (red curve) the aptasensor was treated with Apyrase-treated brain microdialysate. No significant signal change was observed after the aptasensor was treated with Apyrase-treated brain microdialysate, again demonstrating that the aptasensor was selective for ATP detection in brain microdialysate.

4. Conclusions

In summary, we demonstrated that an aptamer superstructure-based electrochemical sensor can be used for highly sensitive and selective detection of ATP in the rat brain. Strong electrochemical signals were generated from the multiple redox molecules (MB) labeled on the aptamer units in the superstructure. In the presence of ATP, considerable signal decrease could be observed owing to the disassembling of the aptamer superstructure from the electrode surface resulting from the strong interaction between ATP and the aptamer units. These merits of aptamer superstructures endow the aptasensor with good sensitivity and high specificity for ATP detection as well as regenerability. The strategy demonstrated here is expected to be versatile for *in vivo* analysis of other physiologically important species in the central nervous system.

Conflicts of interest

There are no conflicts to declare.

Acknowledgements

This work is supported by Beijing Natural Science Foundation (2174088), the National Natural Science Foundation of China (Grant No. 21605147, 21790390 for Y. J.; 21790391, 21435007, 21621062 for L. M.), the National Basic Research Program of China (Grant No. 2016YFA0200104), and the Chinese Academy of Sciences.

Notes and references

1 D. L. Robinson, A. Hermans, A. T. Seipel and R. M. Wightman, *Chem. Rev.*, 2008, **108**, 2554–2584.
2 A. M. Andrews, A. Schepartz, J. V. Sweedler and P. S. Weiss, *J. Am. Chem. Soc.*, 2014, **136**, 1–2.

3 M. Zhang, P. Yu and L. Mao, *Acc. Chem. Res.*, 2012, **45**, 533–543.
4 X. Li, J. Dunevall and A. G. Ewing, *Acc. Chem. Res.*, 2016, **49**, 2347–2354.
5 T. Xiao, F. Wu, J. Hao, M. Zhang, P. Yu and L. Mao, *Anal. Chem.*, 2017, **89**, 300–313.
6 F. Du, X. H. Zhu, Y. Zhang, M. Friedman, N. Zhang, K. Ugurbil and W. Chen, *Proc. Natl. Acad. Sci. U. S. A.*, 2008, **105**, 6409–6414.
7 A. V. Gourine, E. Llaudet, N. Dale and K. M. Spyer, *Nature*, 2005, **436**, 108–111.
8 M. Erecinska and I. A. Silver, *J. Cereb. Blood Flow Metab.*, 1989, **9**, 2–19.
9 A. Cisneros-Mejorado, A. Perez-Samartin, M. Gottlieb and C. Matute, *Cell. Mol. Neurobiol.*, 2015, **35**, 1–6.
10 R. J. Rodrigues, A. R. Tome and R. A. Cunha, *Front. Neurosci.*, 2015, **9**, 148.
11 H. Inoue and K. Tani, *Cell Death Differ.*, 2014, **21**, 39–49.
12 T. Lee, P. Seeman, A. Rajput, I. J. Farley and O. Hornykiewicz, *Nature*, 1978, **273**, 59–61.
13 K. T. Bush, S. H. Keller and S. K. Nigam, *J. Clin. Invest.*, 2000, **106**, 621–626.
14 E. Llaudet, S. Hatz, M. Droniou and N. Dale, *Anal. Chem.*, 2005, **77**, 3267–3273.
15 H. Xie, Y. Chai, Y. Yuan and R. Yuan, *Chem. Commun.*, 2017, **53**, 8368–8371.
16 D. Ji, H. Wang, J. Ge, L. Zhang, J. Li, D. Bai, J. Chen and Z. Li, *Anal. Biochem.*, 2017, **526**, 22–28.
17 G. V. Zyryanov, M. A. Palacios and P. Anzenbacher Jr., *Angew. Chem., Int. Ed.*, 2007, **46**, 7849–7852.
18 P. Yu, X. He, L. Zhang and L. Mao, *Anal. Chem.*, 2015, **87**, 1373–1380.
19 Q. Deng, C. J. Watson and R. T. Kennedy, *J. Chromatogr. A*, 2003, **1005**, 123–130.
20 J. L. He, Z. S. Wu, P. Hu, S. P. Wang, G. L. Shen and R. Q. Yu, *Analyst*, 2010, **135**, 570–576.
21 H. A. Khan, *J. Biosci.*, 2003, **28**, 379–382.
22 A. D. Ellington and J. W. Szostak, *Nature*, 1990, **346**, 818–822.
23 C. Tuerk and L. Gold, *Science*, 1990, **249**, 505–510.
24 M. Famulok, J. S. Hartig and G. Mayer, *Chem. Rev.*, 2007, **107**, 3715–3743.
25 K. Sefah, D. Shangguan, X. Xiong, M. B. O'Donoghue and W. Tan, *Nat. Protoc.*, 2010, **5**, 1169–1185.
26 Q. Wu, Y. Wang, H. Wang, L. Wu, H. Zhang, Y. Song, Z. Zhu, D. Kang and C. Yang, *Analyst*, 2018, **143**, 2267–2275.
27 P. Li, X. Y. Kong, G. Xie, K. Xiao, Z. Zhang, L. Wen and L. Jiang, *Small*, 2016, **12**, 1854–1858.
28 L. R. Schoukroun-Barnes, S. Wagan and R. J. White, *Anal. Chem.*, 2014, **86**, 1131–1137.
29 J. Wang, J. Hou, H. Zhang, Y. Tian and L. Jiang, *ACS Appl. Mater. Interfaces*, 2018, **10**, 2033–2039.
30 R. J. White, N. Phares, A. A. Lubin, Y. Xiao and K. W. Plaxco, *Langmuir*, 2008, **24**, 10513–10518.
31 T. Tokunaga, S. Namiki, K. Yamada, T. Imaishi, H. Nonaka, K. Hirose and S. Sando, *J. Am. Chem. Soc.*, 2012, **134**, 9561–9564.
32 Y. Wu, F. Xiao, Z. Wu and R. Yu, *Anal. Chem.*, 2017, **89**, 2852–2858.
33 J. Zhang, L. P. Smaga, N. S. R. Satyavolu, J. Chan and Y. Lu, *J. Am. Chem. Soc.*, 2017, **139**, 17225–17228.
34 J. Wang, L. Wang, X. Liu, Z. Liang, S. Song, W. Li, G. Li and C. Fan, *Adv. Mater.*, 2007, **19**, 3943–3946.
35 J. Das, K. B. Cederquist, A. A. Zaragoza, P. E. Lee, E. H. Sargent and S. O. Kelley, *Nat. Chem.*, 2012, **4**, 642–648.
36 R. Freeman, X. Liu and I. Willner, *J. Am. Chem. Soc.*, 2011, **133**, 11597–11604.
37 Y. Jiang, M. Shi, Y. Liu, S. Wan, C. Cui, L. Zhang and W. Tan, *Angew. Chem., Int. Ed.*, 2017, **56**, 11916–11920.
38 D. Fan, Q. Zhai, W. Zhou, X. Zhu, E. Wang and S. Dong, *Biosens. Bioelectron.*, 2016, **85**, 771–776.
39 Y. Wang, D. Li, W. Ren, Z. Liu, S. Dong and E. Wang, *Chem. Commun.*, 2008, 2520–2522.
40 M. Ilgu and M. Nilsen-Hamilton, *Analyst*, 2016, **141**, 1551–1568.
41 X. Fang and W. Tan, *Acc. Chem. Res.*, 2010, **43**, 48–57.
42 H. Li, P. Dauphin-Ducharme, N. Arroyo-Curras, C. H. Tran, P. A. Vieira, S. Li, C. Shin, J. Somerson, T. E. Kippin and K. W. Plaxco, *Angew. Chem., Int. Ed.*, 2017, **56**, 7492–7495.
43 X. He, K. Zhang, T. Li, Y. Jiang, P. Yu and L. Mao, *J. Am. Chem. Soc.*, 2017, **139**, 1396–1399.
44 K. Zhang, X. He, Y. Liu, P. Yu, J. Fei and L. Mao, *Anal. Chem.*, 2017, **89**, 6794–6799.
45 Y. Lu, X. Li, L. Zhang, P. Yu, L. Su and L. Mao, *Anal. Chem.*, 2008, **80**, 1883–1890.
46 Y. Lu, N. Zhu, P. Yu and L. Mao, *Analyst*, 2008, **133**, 1256–1260.
47 X. Zhang, C. Song, K. Yang, W. Hong, Y. Lu, P. Yu and L. Mao, *Anal. Chem.*, 2018, **90**, 4968–4071.
48 Y. Jiang, N. Liu, W. Guo, F. Xia and L. Jiang, *J. Am. Chem. Soc.*, 2012, **134**, 15395–15401.
49 Y. Jiang, Y. Feng, J. Su, J. Nie, L. Cao, L. Mao, L. Jiang and W. Guo, *J. Am. Chem. Soc.*, 2017, **139**, 18739–18746.
50 X. Li, T. Zhai, P. Gao, H. Cheng, R. Hou, X. Lou and F. Xia, *Nat. Commun.*, 2018, **9**, 40.
51 F. Xia, R. J. White, X. Zuo, A. Patterson, Y. Xiao, D. Kang, X. Gong, K. W. Plaxco and A. J. Heeger, *J. Am. Chem. Soc.*, 2010, **132**, 14346–14348.
52 Z. Zhu, J. Lei, L. Liu and H. Ju, *Analyst*, 2013, **138**, 5995–6000.
53 N. Xie, S. Liu, X. Yang, X. He, J. Huang and K. Wang, *Analyst*, 2017, **142**, 3322–3332.
54 W. Xu, L. Zhu, X. Shao, K. Huang and Y. Luo, *Biosens. Bioelectron.*, 2018, **120**, 168–174.
55 Y. Xiao, A. A. Lubin, A. J. Heeger and K. W. Plaxco, *Angew. Chem., Int. Ed.*, 2005, **44**, 5456–5459.
56 X. Song, Y. Wang, S. Liu, X. Zhang, H. Wang, J. Wang and J. Huang, *Analyst*, 2018, **143**, 5771–5778.
57 B. Wei, J. Zhang, H. Wang and F. Xia, *Analyst*, 2016, **141**, 4313–4318.
58 S. Guo, H. Yan, F. Wu, L. Zhao, P. Yu, H. Liu, Y. Li and L. Mao, *Anal. Chem.*, 2017, **89**, 13008–13015.